Gelling kinetics and *in situ* mineralization of alginate hydrogels: a correlative spatiotemporal characterization toolbox

Sindre H. Bjørnøy[a], Stefan Mandaric[a], David C. Bassett[a], Andreas K. O. Åslund[a], Seniz Ucar[b], Jens-Petter Andreassen[b], Berit L. Strand[c], Pawel Sikorski[a,*]

[a]*Department of Physics, NTNU, Norwegian University of Science and Technology, 7491 Trondheim, Norway*
[b]*Department of Chemical Engineering, NTNU, Norwegian University of Science and Technology, 7491 Trondheim, Norway*
[c]*Department of Biotechnology, NTNU, Norwegian University of Science and Technology, Trondheim, 7491 Norway*

Abstract

Due to their large water content and structural similarities to the extracellular matrix, hydrogels are an attractive class of material in the tissue engineering field. Polymers capable of ionotropic gelation are of special interest due to their ability to form gels at mild conditions. In this study we have developed an experimental toolbox to measure the gelling kinetics of alginate upon crosslinking with calcium ions. A reaction-diffusion model for gelation has been used to describe the diffusion of calcium within the hydrogel and was shown to match experimental observations well. In particular, a single set of parameters was able to predict gelation kinetics over a wide range of gelling ion concentrations. The developed model was used to predict the gelling time for a number of geometries, including microspheres typically used for cell encapsulation. We also demonstrate that this toolbox can be used to spatiotemporally investigate the formation and evolution of mineral within the hydrogel network via correla-

*Corresponding author
Email addresses: sindre.bjornoy@ntnu.no (Sindre H. Bjørnøy), david.bassett@ntnu.no (David C. Bassett), andreas.aslund@ntnu.no (Andreas K. O. Åslund), seniz.ucar@ntnu.no (Seniz Ucar), jens-petter.andreassen@ntnu.no (Jens-Petter Andreassen), berit.l.strand@ntnu.no (Berit L. Strand), pawel.sikorski@ntnu.no (Pawel Sikorski)

tive Raman microspectroscopy, confocal laser scanning microscopy and electron microscopy.

Keywords: alginate, hydrogel, modeling, raman spectroscopy

1. Introduction

Alginates are a group of biopolymers widely used in biomedical applications and research, largely due to low immunogenicity, low toxicity and ease of forming stable hydrogels under cell compatible and near physiological conditions.[1–8] Alginate hydrogels with different physical forms, often made with encapsulated cells, have been fabricated, including micro- and macro-scale beads, alginate fibers, films, foams and 3D gels.[9–15] Recent research areas of particular interest and innovation include a wide variety of both hard and soft tissue engineering applications as well as cell encapsulation for the treatment of diseases such as diabetes.[16, 17] Chemically modified alginates are also being investigated as extracellular matrix mimics.[18, 19] To be able to design and fabricate new types of hydrogel based biomaterials, including hydrogel composites, a better understanding of the gel formation process and *in situ* modification strategies is needed.[20, 21] When hydrogels are formed from polymers capable of ionotropic gelation, i.e. crosslinking by exogenous inorganic ions, the gel formation is a complex reaction-diffusion process, involving both transport of gelling and non-gelling ions, diffusion of the ungelled polymer and the formation of junction zones. For alginate, a polysaccharide consisting of mannuronic (M) acid and guluronic (G) acid residues, these junction zones consist of aligned polymers with repeating units of the G-monomer, termed the egg-box model.[22, 23] In addition, it has been shown that MG-blocks also form stable junction zones.[24] A detailed understanding of these processes would not only allow for optimization of cell encapsulation, but also enable the formation of gels with complex geometries, such as fibers, films, microbeads and hollow spheres. In addition, if one is able to combine this knowledge with a detailed understanding of *in situ* modification methods, for example by incorporation of solid inorganic com-

ponents, fibrous reinforcement or hydrogel-hydrogel composites, it would open new avenues for development of composite materials for application within tissue engineering and biomedical research and technology.

Modification of hydrogels with calcium phosphate (CaP) minerals to mimic the microenvironment of bone is one strategy to realize new classes of such composite materials.[25–27] We have focused on controlled mineralization of alginate hydrogels *in situ*, in a process which is compatible with cell encapsulation.[28, 29] In such a system, CaP mineral is formed within the hydrogel network at the time of gelling. However the mineral phase undergoes several transformation and maturation steps, and both initial precipitation and subsequent storage will effect the properties of the final CaP phase. Processes such as crystal nucleation and growth within the gel network, solution mediated transformations and local changes in pH induced by gel formation and/or mineral precipitation are important.[30–32] Kinetics of alginate gelling have previously been investigated in non-mineralized systems and this knowledge has been applied to facilitate the formation of alginate structures with different geometries.[33–37] Mikkelsen and Elgsaeter developed a reaction-diffusion model which describes both gel formation kinetics, as well as the density distribution of alginate in calcium-alginate gels formed by the diffusion of gelling ions.[36] Thu *et al.* has estimated that the alginate gel front moves at a velocity of about 100 $\mu m\,min^{-1}$ corresponding to 1.67 $\mu m\,s^{-1}$ when 50 mM $CaCl_2$ solution was used.[35] However high spatial and temporal resolution experimental data is lacking, making progress in better understanding of the process difficult. High spatial and temporal resolution data on the gel front velocity combined with information about polymer concentration profiles, could be implemented in already existing numerical models, which in turn could be used to aid the rational design of hydrogel fabrication processes in other systems and geometries such as mineralized films, cell encapsulation matrices and microfluidic-based fabrication of alginate microbeads and fibers. Extensive knowledge of the gel system would allow for optimal process design. For example, one could maximize cell viability during cell encapsulation in microbeads, fibers or films, by finding the optimal ion concentrations

and gelling times needed to make stable gels, at the same time minimizing cell exposure to potentially detrimental physicochemical conditions.

The situation is even more complex when a mineral phase, such as calcium phosphate, is precipitated within the hydrogel at the time of gelling. The process involves a complex interplay between many aspects, including fluxes of the reaction substrates and gelling ions, ion consumption due to gel formation, supersaturation controlled nucleation and growth of the mineral phase, spatial and temporal evolution of pH and transformation of the mineral phases.[38] A model experimental system in which these process could be studied *in situ*, in real time and with a range of physical methods would allow for a quantitative description of all these process. In the long run, this type of data could be used to construct complex models of the mineralization process, accounting for nucleation, growth and transformation rates of various CaP phases. This goal is however beyond the scope of this contribution, but it remains as a future challenge.

In this work we present an experimental framework for studying the spatially and temporally resolved gelling and *in situ* mineralization of alginate/calcium phosphate composites. To this experimental framework we apply a range of characterization techniques including dark field and confocal microscopy, scanning electron microscopy, and Raman spectroscopy to investigate the kinetics of gel formation and mineralization in real time. We then describe the development of methods to study the interplay between the hydrogel and mineral phases in hitherto undescribed detail.

2. Experimental

Alginate and gelling solution

All chemical reagents were purchased from Sigma-Aldrich, Norway unless otherwise stated. De-ionized water (DIW, 10-15 MΩcm) was used in all of the experiments. Sodium alginate (*Laminaria hyperborea*, Protanal LF 200S, M_W=2.74×10^5 g mol^{-1}, FMC BioPolymer AS, fraction of G-monomers: F_G =

0.68, F_{GG} = 0.57 and F_{GM} = 0.11) was used in the entire work, except for the alginate labelled with Fluoresceinamine (*Laminaria hyperborea*, Protanal SF60, M_W=2.2×10^5 g mol^{-1}, FMC BioPolymer AS, fraction of G-monomers: F_G = 0.67, F_{GG} = 0.58, F_{GGG} = 0.52) The fluorescently labelled alginate was made as described by Strand *et al.*[39]

Stock solutions of 1 M $CaCl_2$ and 1 M $CaCl_2$ and 0.9 % (w/v) NaCl (VWR) were made in DIW. Buffering was done with 25 mM 3-(N-Morpholino) propanesulfonic acid (MOPS) at pH 6.5 and 7.4 for the gelling experiments and with 50 mM Tris(hydroxymethyl) aminomethane (TRIS) and 50 mM sodium acetate (NaAc) for mineralization experiments at pH 7 and 5 respectively. Gelling experiments refer to experiments where alginate solutions without a phosphate precursor have been used. Mineralization experiments refer to experiments where alginate solutions containing a phosphate precursor have been used. In all cases, gelling solution refers to a solution containing $CaCl_2$. The concentration of calcium and the pH in the gelling solution is specified where necessary.

For the gelling experiments, 2 % (w/v) alginate solution was prepared by dissolving sodium alginate in DIW. For the mineralization experiments 1.8 % alginate solutions containing 0.9 % NaCl, with either 200 mM or 300 mM phosphate were prepared by dissolving sodium alginate and a mixture of $Na_2HPO_4 \cdot 7\,H_2O$ and $NaH_2PO_4 \cdot 2\,H_2O$ (Thermo Fisher Scientific). The ratio of the phosphate precursors were chosen to give a final pH between 5 and 7. All sodium alginate solutions were stored at 4 °C between experiments.

Alginate flow cells

In order to conduct the experiments, a simple flow cell was constructed. The flow cell consisted of an alginate droplet sandwiched between two microscope slides separated by strips of 140 µm thick double-sided tape. A 1.5 µL droplet of alginate solution was placed onto the centre of the slide and covered by either a second microscope slide or a cover slip as shown in Figure 1 a. Gentle pressure was applied in order to compress the droplet into a disc. 150 µL of gelling solution was then applied into the spacing between the slides to initiate the

gelling.

Dark-field microscopy

The gelling reaction was studied in an Olympus IX-70 Inverted Microscope. The objective used was Olympus UPlanFl 4x/0.13NA in combination with a Ph1 condenser annulus. This objective did not have a phase ring which lead to a non-traditional contrast mechanism provided by a mixture of phase contrast and dark-field contrast. However, the settings were chosen on purpose, as this mode provided the best contrast for observation of the moving gel front. A high speed camera (Photron SA-3) connected to the microscope side port filmed the gelling. The gel front velocity was determined from the videos using a custom developed script and MATLAB (R2014b). Briefly, the Canny edge detector operator with low threshold was used to detect the gel front, producing a binary image of all high contrast features in the image. The gel front was isolated by excluding all static features and all edges below a threshold size and was then fitted with an ellipse. The gel front radius was calculated by averaging the two ellipse axes. All samples were close to circular. The gel front position was plotted as a function of time, and the gel front velocity was found by calculating the slope of the linear region of the resulting plot.

Confocal laser scanning microscopy

The gelling of Fluoresceinamine-labelled alginate was performed in the flow cells described above and observed with a Leica TCS SP5 Confocal Laser Scanning Microscope (CLSM). A Leica HCX PL FLUOTAR 5.0x/0.15NA dry objective was used in combination with argon laser 488 nm line. The resulting time series were analyzed in MATLAB.

pH measurements with CLSM

In addition to measurements of the gel front, CLSM was also used in combination with a pH-sensitive dye to measure the local pH. Rhodamine 6 and ethylenediamine was refluxed in methanol for 6 h resulting in a pH-sensitive

fluorescent molecule, named R6G-EDA, according to previous reports.[40, 41] R6G-EDA was used at a concentration of 20 µM in both the alginate- and the gelling-solutions. Sulfhorhodamine 101 (SR101), a pH-insensitive dye, was added to give a concentration of 5 µM to both solutions. An argon laser (LASOS LGK 7872 ML05, wavelength 514 nm) and a diode pumped solid state laser (LASOS DPSS, wavelength 561 nm) were scanned sequentially line by line in order to avoid cross-talk between the two dyes. Emission filters at 525-555 nm and 575-625 were used for R6G-EDA and SR101, respectively. The lasers were set at the same intensity in the measurements as during the calibration, and low noise Leica HyD detectors were used in photon counting mode. The scan speed was set at 100 Hz, which, with a resolution of 256x256 pixels, limited the temporal resolution of the pH measurements to 0.1 frame per second. A 3x3 pixel median filter was applied to the images and the ratio between the R6G-EDA images and SR101 images was calculated for each pixel. This ratio was converted to a pH-value by comparison with a standard curve based on measurements of known pH-values of the calcium-solution. The standard curve was made based on eight samples of known pH. The samples contained 1 M $CaCl_2$, 0.9 % NaCl, 20 µM R6G-EDA, 5 µM SR101 and either 50 mM sodium acetate or TRIS buffer and ranged from pH 4 to 7.5 in 0.5 intervals. Three images were recorded at different locations for each of the eight pH values, and pixel ratios were found as described above. The SR101/R6G-EDA-ratio was used for pH-values above pH 5.5 while the R6G-EDA/SR101-ratio was used for pH-values below 5.5. The measured intensity ratios were fitted with a fourth degree polynomial for SR101/R6G-EDA and a seventh degree polynomial for R6G-EDA/SR101. The measurements and resulting fits can be seen in Figure S.1 a in the Supplementary Info. These curves were then used to convert the intensity ratio in an image pixel into a pH value. Figure S.2 b in the Supplementary Info shows a correlation plot of the known pH-values vs. the measured pH with the method described.

Raman microspectroscopy

Raman microspectroscopy was performed using a Renishaw InVia Reflex Spectrometer equipped with a 532 nm laser (RL532C100) through a Leica 10X 0.25NA lens. The flow cell for these experiments was made in the same way as described earlier, although the regular microscope slides were replaced with Raman grade CaF_2-slides from Crystran Ltd, UK (see Figure S.2). Spatial information was obtained by collecting measurements while scanning the laser across the hydrogel discs. Line scans were performed by scanning 50 points along the radius of hydrogel discs, resulting in one point approximately every 15 µm. 10 spectra were collected for 3 s each and co-added to produce a single spectrum for each point. Database samples for Raman analysis of brushite (DCPD), octacalcium phosphate (OCP) and hydroxyapatite (HAp) were prepared according to methods described by Elliott and phase purity was confirmed with powder X-ray diffraction (D8 Advance DaVinci, Bruker AXS) prior to Raman measurements, see Figure S.3.[42]

Scanning electron microscopy

For scanning electron microscopy (SEM) studies, the samples made in the flow cell were rinsed with DIW after a given time inside the flowcell. The flowcell was separated and the alginate discs were dehydrated in increasing concentrations of ethanol and critical point dried using CO_2 (Emitech K850 critical point dryer). Dried samples were attached to SEM stubs with carbon tape and sputter coated (Cressington 208 HR) with 5 nm platinum/palladium (80/20). Imaging was performed with an accelerating voltage between 1 and 10 kV (Hitachi S-5500 S(T)EM).

Numerical solution of gelling model

Numerical modeling of the gelling process was based on a simple reaction-diffusion model originally proposed by Mikkelsen-Elgsaeter and an alginate-calcium interaction scheme commonly referred to as the egg-box model.[22, 34,

36] Combined with adjustments for calcium binding stoichiometry proposed by Thu *et al.* the following system of differential equations have been obtained:[35]

$$\frac{\partial c}{\partial t} = D_c \nabla^2 c - N_c \frac{\partial g}{\partial t} \tag{1}$$

$$\frac{\partial a}{\partial t} = \nabla [D_a \nabla a] - \frac{\partial g}{\partial t} \tag{2}$$

$$\frac{\partial g}{\partial t} = kca^2 + kcag \tag{3}$$

Here, c, a, and g are the total concentration of calcium, ungelled alginate and gelled alginate, respectively (c and a are given as the concentration of alginate monomers, equivalent to the molar concentration of carboxyl groups). D_c and D_a are the diffusion constants for calcium ions and ungelled alginate molecules. N_c is a stoichiometric coefficient describing the number of calcium-ions per alginate-dimer, dependent on both the guluronic acid content of the alginate as well as the affinity between calcium ions and alginate blocks. Finally, in this model k is an effective reaction rate constant.[36] The model has in principle four adjustable parameters: N_c, D_c, D_a, k, in addition to the $CaCl_2$ and alginate concentrations which were determined by the experimental conditions.

The system of differential equations was solved numerically in MATLAB using the built-in solver `pdepe` for one dimensional parabolic-elliptic partial differential equations. In all cases, 1000 time steps were used and an evenly spaced grid of 2000 points was used for the spatial dimension along the radius of an alginate cylinder or alginate sphere for which the gel front position as a function of time was calculated. The reaction-diffusion model was solved in cylindrical or spherical coordinate system using the option of the `pdepe` solver for disc and sphere geometries respectively.

Comparison between the gel front position predicted by the model and observed experimentally was used to determine the adjustable parameters in the model. Previously reported values of the diffusion constant for calcium ions in free solution of 0.78 $\times 10^{-9}$ $m^2\,s^{-1}$ was used for D_c[43]. The diffusion of Ca^{2+}

in the alginate gel is largely unaffected by the gel network since the diffusion of molecules with a molecular weight below 2×10^4 g mol^{-1} are expected to behave the same as in free solution.[44] A diffusion constant for ungelled alginate of 1×10^{-11} m^2 s^{-1} was used, since the gel front kinetics do not strongly depended on the diffusion constant of alginate.[34] The two remaining parameters of the model N_C and k were determined by fitting the predicted gelling kinetics to the experimental data and calculating the root-mean-square error. A systematic search through the parameter space was used in order to exclude local minima.

3. Results and discussion

Kinetics of alginate gel formation

The design of the flow cell is shown in Figure 1 a. Figure 1 b and c illustrate the processes that can be studied in the flow cell system. In the first instance we investigated the kinetics of alginate gel formation in order to verify the experimental design and to investigate the dependence of gel formation kinetics on gelling ion concentration, pH and the presence of additives such as NaCl. Following introduction of the calcium solution to the flow cell, the gel front could be observed both in dark field (DF) microscopy (Figure 2) as well as in CLSM when fluorescently labeled alginate was used (Figure 3). In DF microscopy, the gel front was visible as a narrow bright band and significant contrast between gelled and ungelled alginate was observed, presumably due to the difference in refractive index for the two conditions. In CLSM the gel front was visible as a narrow region with reduced fluorescence (depletion zone) as shown in Figure 3. The origin of that depletion zone is described below and has also been observed previously.[34]

For DF microscopy, a series of images were recorded and analyzed to determine the velocity of the gel front, see Figure 2 a. The position of the gel front was determined using a custom MATLAB script and was plotted as a function of time, see Figure 2 b. To compare gelling kinetics for different experimental conditions, the slope of the linear region in a plot of the front position versus

time was used. The advantage of our experimental system is a well defined cylindrical geometry, with a flux of gelling ions only along the radial coordinate. The alginate and gel concentrations, as well as the concentrations of gelling and non-gelling ions was uniform along the direction parallel to the flow cell normal. For this sample geometry, the gel front velocity in the linear region was measured to increase from approximately 1 µm s^{-1} up to 4.5 µm s^{-1} when the calcium concentration was increased from 50 mM to 1 M, respectively, see Figure 2 c. The gel front velocity determined from the position of the depletion zone observed in CLSM when using a fluorescently labeled alginate corresponded well to that determined by DF microscopy (Figure 3 b). This confirms that both techniques allowed direct observation of the gel front. It is therefore straightforward to investigate the influence of other experimental parameters on the gel front kinetics, such as pH and ionic strength. Using the setup described above, we have found that the gel front velocity was not substantially dependent on the addition of NaCl (see Figure S.4 a). The largest difference was observed for 1 M $CaCl_2$, where the gel front velocity was increased from 4.4 µm s^{-1} to 4.9 µm s^{-1} upon addition of 0.9 % NaCl. High salt concentration is expected to lower the binding between alginate and Ca^{2+} ions due to increased screening and competition with the Na^+ ions, which in turn should increase the gel front velocity. No difference was found for unbuffered samples (pH ∼7) and samples buffered at pH 6.5 and 7.4, see Figure S.4 b.

The results obtained for disc geometries cannot be directly compared with literature values measured for spherical geometries, as the sample geometry affects the flux of ions to the gel core, and the front velocity is different for the two cases. However, our results allow for the development of a gelling model which can be used to predict gelling kinetics for spherical geometries from the parameters determined for cylindrical geometries (see below for a more detailed description of the modeling strategy). The observed gel front velocity in a disc geometry recalculated to a spherical geometry and experimental conditions as used by Thu *et al.* (50 mM $CaCl_2$, d=4 mm, 1.8% alginate solution), gives the velocity in the linear region equal to 1.1 µm s^{-1}. The average velocity for the

whole gelling process and not only for the linear region for this sample size, geometry, and ionic strength was herein calculated to be 1.4 µm s^{-1}, which is in good agreement with the estimate of 1.7 µm s^{-1} based on low resolution optical microscopy in the work of Thu *et al.*[35]

Modeling

Experimental data was used to construct a quantitative description of the gelling process by fitting the observed, time dependent gel front position to those predicted from the reaction-diffusion model described above. The model has 4 adjustable parameters, namely the diffusion constants for ungelled alginate and calcium ions D_a and D_c, the reaction rate for egg-box formation k and the Ca^{2+} binding stoichiometry coefficient N_c.[34, 36] As described in materials and methods, literature values for D_c and D_a were used here. The two remaining parameters of the model, N_c and k, were determined by comparing the predicted gelling kinetics with experimental data. We started by determining the values of the two model parameters using gel front position data from an experiment using 1 M $CaCl_2$ solution. As illustrated in Figure 4 a, excellent agreement between the observed and modeled gel front positions was obtained for $k \geq 275$ M^{-2} s^{-1}, $N_c = 0.30$ at 1 M $CaCl_2$. We found that all models with k larger than this lower boundary value could explain the experimental data. This clearly indicates that the gel front velocity is limited by the diffusion of ions and not by reaction kinetics. If the proposed modeling approach is correct, the model should be able to predict gel front position as a function of time for samples with other concentrations of $CaCl_2$ without recourse to modify any other model parameters. Indeed, good agreement between the observed and predicted gel front position for all investigated $CaCl_2$ concentrations down to 50 mM was observed. The agreement is excellent for 750 mM, 500 mM and 250 mM. For the two lowest concentrations (100 mM and 50 mM) the model predicts the correct slope (velocity of the gel front), but the experimental curve is slightly offset with respect to that predicted by the model (Figure 4 a). However, it is important to note that for the two lowest concentrations tested, the gel front

was more difficult to observe in the optical techniques used here and its absolute position might be subject to a larger systematic error. This is a likely cause of the slight discrepancy in the calculated gel front velocity between the work of Thu *et al.* and the results presented here.

We also note that our experimental system could be used to precisely determine the diffusion constant of alginate during gel formation at various conditions using CLSM, fluorescently labeled alginate and the shape and intensity reduction in a clearly visible depletion zone by applying, for example, the theoretical framework presented recently by Braschler *et al.*[34] This is, however, beyond the scope of the current work and would serve as an interesting addition. This approach could also be used to study the reaction constant k for different types of alginates or reaction with various divalent cations in great detail.

As described by Braschler *et al.* the determined N_c parameter is closely related to the fraction of G-units of alginate, assuming that only G-units are able to bind Ca^{2+} ions and that the binding is independent of the sequence of G and M units.[34] In practice, it is known that divalent cation binding by G-blocks in alginate is cooperative, and a longer stretch of consecutive G-units is needed to form stable junction zones.[22] It has also been shown that MG-sequences bind Ca^{2+}.[24] We can use our measured value for N_c to estimate the apparent fraction of G-units that rapidly binds calcium during the initial gel formation step, F_G^*. F_G^* is still related to the stoichiometry in the egg-box model and is given as:[45]

$$F_G^* = \frac{4}{3} N_c$$

Using the equation above, F_G^* was calculated to be 0.4 and this is based only on the amount of Ca^{2+} ions consumed during the gelling process. Note that this experiment has only considered alginate sequences with the highest affinity for Ca^{2+} ions, and it is likely that more Ca^{2+} ions are bound to the polymer as the gel matures.[23, 46] This cooperative binding i.e. blocks of G-monomers will bind Ca^{2+} faster than single G-monomers, is a probable reason for the discrepancy between the calculated F_G^*=0.4 and the F_G=0.67 given by the manu-

facturer.

The predicted temporal evolution of the gel front is illustrated in Figure 4 b where the gelled alginate concentration profiles (green line) and the total alginate (orange line) are plotted at 40 s intervals (these concentrations refer to alginate monomers, not alginate molecules). Here a depletion zone is clearly seen moving towards the center of the disc (at $r = 0$), which is consistent with observations made by CLSM. The origin of this depletion zone is illustrated more clearly in Figure 4 c and d where the predicted concentration profiles for Ca^{2+} (blue), ungelled (red), gelled (green) and total alginate (orange) at 240 s and 720 s after the gelling was initiated are shown. Gelling is predicted to be confined to a small region of approximately 200 µm, where the solution rapidly transitions from an ungelled Na-alginate sol to gelled Ca-alginate gel.

Figure 5 a shows the developed model applied to the prediction of gelling kinetics for two different geometries of alginate sample, discs and spheres, as a function of $CaCl_2$ concentration. Here, the diameter of both geometries was set to 500 µm which represents a typical size of an alginate bead used for cell encapsulation. The model predicts that at a concentration of 50 mM $CaCl_2$, the time needed to fully gel such a bead is approximately 20 s; the gelling time is reduced to 15 s and 5s for 100 and 1000 mM $CaCl_2$ respectively.

Figure 5 b illustrates a simulation in which the gelling model was applied to predict how gelling would occur when an alginate fiber is produced in a coaxial flow microfluidic device.[10, 47] Here, we have simulated a central alginate stream with a circular cross-section and a diameter of 200 µm which contacts the gelling solution from both sides and flows to the right with the same velocity at $t = 0$. The alginate and gelling stream flow together and Ca^{2+} diffuses into the alginate causing gel formation. Gelling begins along the fiber edges and after approximately 600 ms a shell of gelled alginate has formed around the fiber. After 3.5 s, 50 % of the alginate in the fiber core is gelled and a fully gelled fiber is formed after approximately 7.5 s. Some residual inhomogeneity with respect to the gelled alginate concentration in the fibers is observed with the lowest concentration in the center, which is comparable to the sphere and

disc geometries. Depending on the flow rate, this can be used to calculate the length of the channel where gelling occurs in a microfluidic device.

Mineralization

By introducing a phosphate precursor into the alginate solution, precipitation of calcium phosphate mineral may occur at the same time as the gel is formed following addition of Ca^{2+}. As illustrated in Figure 6, deposition of the mineral phase could be directly observed using optical microscopy. Here, the alginate solution contains 300 mM of sodium phosphate. The formed mineral phase was typically visible as an opaque, light scattering region close to, but trailing slightly behind the gel front. Interestingly, the appearance of this region was not constant, but appeared to change with time, within both short (i.e. minutes) and long (i.e. tens of hours) time scales.

It is known that CaP crystallization might cause local changes in the pH of the sample due to different stoichiometry of CaP phases. To investigate this aspect of the mineralization process, CLSM in combination with two fluorescent dyes was used. The dye R6G-EDA is known to have an increasing fluorescence intensity as the degree of protonation increases and has a detectable fluorescence from pH 7.5 and accurate measurements of pH changes can be made between pH 4-6.[41] We also applied a pH-insensitive dye, SR101, in order to correct for artifacts in fluorescence intensity measurements which may occur due to dilution, sample thickness, uneven illumination and scattering from mineral formation. This combination of dyes gave excellent sensitivity to pH in the range of pH 4-6.5, see Figure S.1.

Figure 7 shows bright field and R6G-EDA/SR101 ratio images of two mineralizing samples at different time points. For the sample marked pH 5, the alginate disc was buffered at pH 7 due to the phosphate content and the surrounding calcium solution was buffered at pH 5. As mineral precipitated and the surrounding solution diffused into the alginate disc, the pH was lowered. For this sample, the gelling process was completed after 300 s, however the pH continued to drop and reached a minimum of 4.4 in the center of the disc after

approximately 18 min. The sample marked pH 7 was made in a similar manner except that the gelling solution was buffered at pH 7. Here the increased fluorescence intensity was entirely due to H^+ produced during the mineralization process. This sample also showed the same trend with the lowest pH observed at the center of the disc. The pH in the center of the disc was found to drop to 4.5 after approximately 20 min. Once the pH had reached this minimum it was stable in the center of the disc for the rest of the measurement which, in both cases, lasted 33 min in total. A probable cause was the consumption of the buffer agent (phosphate buffer) within the discs in the mineralization process, resulting in a pH-gradient as the buffer agent in the surrounding solution (TRIS or sodium acetate) diffused into the gelling disc. This gradient persisted throughout the duration of the experiments.

The sample geometry allowed for *in situ* monitoring of the mineral formation and transformation using confocal Raman microspectroscopy (CRM). This is especially important, as dehydration needed for characterization using powder X-ray diffraction (XRD) or electron diffraction techniques might introduce changes in the mineral phase. Also, due to small sample size, characterization, particularly using XRD, is challenging. Figure 8 a shows Raman spectra of several minerals and species of interest for our mineralized alginate composite, including HAp, OCP, brushite, alginate and alginate-phosphate precursor solution. Figure 8 b shows a heat map generated by collecting Raman spectra in a radial direction across a mineralized alginate disc. Here the data was collected from a sample which was prepared with alginate containing 300 mM phosphate and gelled in 1 M $CaCl_2$ buffered at pH 5 with sodium acetate. In the region close to the disc edge, an intense signal located at 958 cm^{-1}, corresponding to OCP was recorded. In the region of interest, the OCP Raman spectrum consists of a main peak at 958 cm^{-1} and a distinct shoulder at 967 cm^{-1}.[48] There is also a characteristic (but weak) HPO_4-stretch located at 1010 cm^{-1}, however, this peak was close to the background level in the used experimental conditions. The peak shape of HAp is more symmetrical (although there is a slight shoulder at lower wavenumbers, i.e. the other side than the OCP-shoulder) and via curve-

fitting the two phases can be distinguished using Raman microspectroscopy.[49] A weaker signal from the alginate itself was also observed at 816 and 890 cm^{-1} as well as a broad peak from the acetate buffer at 932 cm^{-1}. The signal from alginate and buffer were unchanged throughout the radius of the disc, while the signal from the mineral was strong towards the edge and gradually diminished towards the center of the disc. No mineral was detected in a radius of 250 µm from the center of the disc.

The morphology of the formed mineral phase was investigated at high resolution using SEM after careful drying of the samples. SEM could also be applied to the same sample as CRM, therefore allowing highly accurate phase identification combined with high magnification imaging of the same area. Figure 8 c shows example images of a mineralised alginate sample, showing the difference in mineral content and morphology at different areas of the disc: at the center (1), halfway to the edge (2) and at the edge (3). Their corresponding positions are marked in Figure 8 b. In the center, no mineral was observed, corroborating the CRM measurements described earlier. Further towards the edge of the sample, mineral platelets were dispersed in the alginate network. Close to the edge of the disc, a large abundance of acicular crystals were found. The images in Figure 8 c correspond to positions 50, 450 and 600 µm respectively in Figure 8 b. The combination of these techniques can also be used to study mineral phase transformations within the hydrogel, and this concept is studied in detail elsewhere.[49]

4. Conclusion

In summary, we have developed an experimental platform in which the gelling kinetics of polymers capable of ionotropic gelation can be studied with high spatial and temporal resolution. The gel front velocity for 1.8 % high G-content alginate gel was measured at a range of condition with both transmitted light and fluorescence microscopy. For the disc geometry investigated in this study, this velocity ranged from 1 to 5 $\mu m\, s^{-1}$ for $CaCl_2$ concentrations

between 50 mM and 1 M. Modeling of the gel formation process based on a reaction-diffusion approach was implemented and the gelling front velocity was calculated for a range of geometries and $CaCl_2$ concentrations. The calculated values are in excellent agreement with measured or previously published data. The same platform was combined with several other analytical techniques such as confocal Raman microspectroscopy, confocal laser scanning microscopy and scanning electron microscopy to obtain temporally and spatially resolved information regarding the chemical composition, polymer concentration, evolution of pH and sub-micron morphology of regions of interest. This is especially suitable for characterization of *in situ* mineralization processes of a hydrogel system, here demonstrated by mineralization of alginate with calcium phosphate. The presented platform represents a powerful new characterization toolbox to undertake studies of gelling kinetics, *in situ* mineral formation and maturation behavior within hydrogels in exquisite detail.

5. Acknowledgments

The authors thank the Research Council of Norway FRINATEK project 214607 and NANO2021 project 220005 (A.K.O.Å.) for financial support.

References

[1] A. Steinbüchel (Ed.), Biopolymers Online, Wiley-VCH Verlag GmbH & Co. KGaA, Weinheim, Germany, 2005.

[2] B. H. A. Rehm (Ed.), Alginates: Biology and Applications, Vol. 13 of Microbiology Monographs, Springer Berlin Heidelberg, Berlin, Heidelberg, 2009.

[3] Y. A. Mørch, I. Donati, B. L. Strand, G. Skjåk-Braek, Molecular engineering as an approach to design new functional properties of alginate., Biomacromolecules 8 (9) (2007) 2809–14.

[4] K. B. Fonseca, D. B. Gomes, K. Lee, S. G. Santos, A. Sousa, E. A. Silva, D. J. Mooney, P. L. Granja, C. C. Barrias, Injectable MMP-sensitive alginate hydrogels as hMSC delivery systems., Biomacromolecules 15 (1) (2014) 380–90.

[5] K. Y. Lee, D. J. Mooney, Hydrogels for tissue engineering., Chem Rev 101 (7) (2001) 1869–1879.

[6] J. E. Melvik, M. Dornish, Alginate as a carrier for cell immobilisation, in: Focus Biotechnol. vol. 8A Fundam. Cell Immobil. Biotechnol., Kluwer Academic Press, 2004, pp. 165–183.

[7] E. Alsberg, K. W. Anderson, A. Albeiruti, R. T. Franceschi, D. J. Mooney, Cell-interactive alginate hydrogels for bone tissue engineering, J. Dent. Res. 80 (11) (2001) 2025–2029.

[8] G. Chan, D. J. Mooney, New materials for tissue engineering: towards greater control over the biological response, Trends Biotechnol. 7 (2008) 382–392.

[9] A. M. Rokstad, I. Donati, M. Borgogna, J. Oberholzer, B. L. Strand, T. Espevik, G. Skjåk-Braek, Cell-compatible covalently reinforced beads obtained from a chemoenzymatically engineered alginate., Biomaterials 27 (27) (2006) 4726–37.

[10] S.-J. Shin, J.-Y. Park, J.-Y. Lee, H. Park, Y.-D. Park, K.-B. Lee, C.-M. Whang, S.-H. Lee, "On the fly" continuous generation of alginate fibers using a microfluidic device., Langmuir 23 (17) (2007) 9104–9108.

[11] S. Sugiura, T. Oda, Y. Aoyagi, M. Satake, N. Ohkohchi, M. Nakajima, Tubular gel fabrication and cell encapsulation in laminar flow stream formed by microfabricated nozzle array., Lab Chip 8 (8) (2008) 1255–1257.

[12] R. Pereira, A. Carvalho, D. C. Vaz, M. H. Gil, A. Mendes, P. Bártolo, Development of novel alginate based hydrogel films for wound healing ap-

plications., International journal of biological macromolecules 52C (2012) 221–230.

[13] T. Huq, S. Salmieri, A. Khan, R. a. Khan, C. Le Tien, B. Riedl, C. Fraschini, J. Bouchard, J. Uribe-Calderon, M. R. Kamal, M. Lacroix, Nanocrystalline cellulose (NCC) reinforced alginate based biodegradable nanocomposite film., Carbohydrate polymers 90 (4) (2012) 1757–63.

[14] T. Andersen, J. E. Melvik, O. Gåserød, E. Alsberg, B. E. Christensen, Ionically gelled alginate foams: physical properties controlled by operational and macromolecular parameters., Biomacromolecules 13 (11) (2012) 3703–10.

[15] K. Pataky, T. Braschler, A. Negro, P. Renaud, M. P. Lutolf, J. Brugger, Microdrop Printing of Hydrogel Bioinks into 3D Tissue-Like Geometries., Advanced materials (Deerfield Beach, Fla.) (2011) 391–396.

[16] T. Andersen, B. L. Strand, K. Formo, E. Alsberg, B. E. Christensen, Chapter 9.

[17] J. Sun, H. Tan, Alginate-Based Biomaterials for Regenerative Medicine Applications, Materials (Basel). 6 (4) (2013) 1285–1309.

[18] J. A. Rowley, D. J. Mooney, Alginate type and RGD density control myoblast phenotype, J. Biomed. Mater. Res. 60 (2) (2002) 217–223.

[19] O. Chaudhuri, L. Gu, D. Klumpers, M. Darnell, S. A. Bencherif, J. C. Weaver, N. Huebsch, H.-P. Lee, E. Lippens, G. N. Duda, D. J. Mooney, Hydrogels with tunable stress relaxation regulate stem cell fate and activity., Nat. Mater. 15 (3) (2015) 326–334.

[20] M. J. Webber, E. A. Appel, E. W. Meijer, R. Langer, Supramolecular biomaterials, Nat. Mater. 15 (1) (2015) 13–26.

[21] A. Memic, H. A. Alhadrami, M. A. Hussain, M. Aldhahri, F. Al Nowaiser, F. Al-Hazmi, R. Oklu, A. Khademhosseini, Hydrogels 2.0: improved prop-

erties with nanomaterial composites for biomedical applications., Biomed. Mater. 11 (1) (2015) 014104.

[22] G. T. Grant, E. R. Morris, D. A. Rees, P. J. Smith, D. Thom, Biological interactions between polysaccharides and divalent cations: The egg-box model, FEBS Lett. 32 (1) (1973) 195–198.

[23] M. Borgogna, G. Skjåk-Bræk, S. Paoletti, I. Donati, On the initial binding of alginate by calcium ions. The tilted egg-box hypothesis., J. Phys. Chem. B 117 (24) (2013) 7277–82.

[24] I. Donati, S. Holtan, Y. A. Mørch, M. Borgogna, M. Dentini, G. Skjåk-Braek, New hypothesis on the role of alternating sequences in calcium-alginate gels., Biomacromolecules 6 (2) (2005) 1031–40.

[25] D. W. Green, I. Leveque, D. Walsh, D. Howard, X. B. Yang, K. Partridge, S. Mann, R. O. C. Oreffo, Biomineralized polysaccharide capsules for encapsulation, organization, and delivery of human cell types and growth factors, Adv. Funct. Mater. 15 (6) (2005) 917–923.

[26] Z. A. C. Schnepp, R. Gonzalez-McQuire, S. Mann, Hybrid biocomposites based on calcium phosphate mineralization of self-assembled supramolecular hydrogels, Adv. Mater. 18 (14).

[27] M. Xie, M. Ø. Olderøy, J.-P. Andreassen, S. M. Selbach, B. L. Strand, P. Sikorski, Alginate-controlled formation of nanoscale calcium carbonate and hydroxyapatite mineral phase within hydrogel networks, Acta Biomater. 6 (9) (2010) 3665–3675.

[28] M. Xie, M. Ø. Olderøy, Z. Zhang, J.-P. Andreassen, B. L. Strand, P. Sikorski, Biocomposites prepared by alkaline phosphatase mediated mineralization of alginate microbeads, RSC Adv. 2 (4) (2012) 1457.

[29] S. H. Bjørnøy, D. C. Bassett, S. Ucar, J.-P. Andreassen, P. Sikorski, Controlled mineralisation and recrystallisation of brushite within alginate hydrogels., Biomed. Mater. 11 (1) (2016) 015013.

[30] H. Treml, H.-H. Kohler, Coupling of diffusion and reaction in the process of capillary formation in alginate gel, Chemical Physics 252 (1-2) (2000) 199–208.

[31] F. Abbona, H. Madsen, R. Boistelle, The initial phases of calcium and magnesium phosphates precipitated from solutions of high to medium concentrations, Journal of Crystal Growth 74 (3) (1986) 581–590.

[32] S. Ucar, S. H. Bjørnøy, D. C. Bassett, B. L. Strand, P. Sikorski, J.-P. Andreassen, Nucleation and Growth of Brushite in the Presence of Alginate, Cryst. Growth Des. 15 (11) (2015) 5397–5405.

[33] H.-S. Kim, A kinetic study on calcium alginate bead formation, Korean J. Chem. Eng. 7 (1) (1990) 1–6.

[34] T. Braschler, A. Valero, L. Colella, K. Pataky, J. Brugger, P. Renaud, Link between Alginate Reaction Front Propagation and General Reaction Diffusion Theory, Anal. Chem. 83 (6) (2011) 2234–2242.

[35] B. Thu, O. Gåserød, D. Paus, A. Mikkelsen, G. Skjåk-Bræk, R. Toffanin, F. Vittur, R. Rizzo, Inhomogeneous alginate gel spheres: An assessment of the polymer gradients by synchrotron radiation-induced x-ray emission, magnetic resonance microimaging, and mathematical modeling, Biopolymers 53 (1) (2000) 60–71.

[36] A. Mikkelsen, A. Elgsaeter, Density distribution of calcium-induced alginate gels. A numerical study, Biopolymers 36 (1) (1995) 17–41.

[37] O. Bonhomme, J. Leng, A. Colin, Microfluidic wet-spinning of alginate microfibers: a theoretical analysis of fiber formation, Soft Matter 8 (41) (2012) 10641.

[38] S. Mann, Biomineralization Principles and Concepts in Bioinorganic Materials Chemistry, Oxford Univ Press, 2001.

[39] B. L. Strand, Y. A. Morch, K. R. Syvertsen, T. Espevik, G. Skjak-Braek, Microcapsules made by enzymatically tailored alginate, J. Biomed. Mater. Res. 64A (3) (2003) 540–550.

[40] J.-S. Wu, I.-C. Hwang, K. S. Kim, J. S. Kim, Rhodamine-based Hg2+-selective chemodosimeter in aqueous solution: fluorescent OFF-ON., Organic letters 9 (5) (2007) 907–10.

[41] Z. Li, S. Wu, J. Han, S. Han, Imaging of intracellular acidic compartments with a sensitive rhodamine based fluorogenic pH sensor., The Analyst 136 (2011) 3698–3706.

[42] J. Elliott, Structure and Chemistry of the Apatites and Other Calcium Orthophosphates, Elsevier B.V., 1994.

[43] J. H. Wang, Tracer-diffusion in Liquids. IV. Self-diffusion of Calcium Ion and Chloride Ion in Aqueous Calcium Chloride Solutions 1, J. Am. Chem. Soc. 75 (7) (1953) 1769–1770.

[44] A. Martinsen, I. Storrø, G. Skjårk-Braek, Alginate as immobilization material: III. Diffusional properties., Biotechnol. Bioeng. 39 (2) (1992) 186–94.

[45] E. R. Morris, D. A. Rees, D. Thom, J. Boyd, Chiroptical and stoichiometric evidence of a specific, primary dimerisation process in alginate gelation, Carbohydr. Res. 66 (1) (1978) 145–154.

[46] Y. Fang, S. Al-Assaf, G. O. Phillips, K. Nishinari, T. Funami, P. A. Williams, L. Li, Multiple steps and critical behaviors of the binding of calcium to alginate., J. Phys. Chem. B 111 (10) (2007) 2456–62.

[47] H. Onoe, T. Okitsu, A. Itou, M. Kato-Negishi, R. Gojo, D. Kiriya, K. Sato, S. Miura, S. Iwanaga, K. Kuribayashi-Shigetomi, Y. T. Matsunaga, Y. Shimoyama, S. Takeuchi, Metre-long cell-laden microfibres exhibit tissue morphologies and functions., Nature materials 12 (6) (2013) 584–590.

[48] B. O. Fowler, M. Markovic, W. E. Brown, Octacalcium phosphate. 3. Infrared and Raman vibrational spectra, Chemistry of Materials 5 (10) (1993) 1417–1423.

[49] S. H. Bjørnøy, D. C. Bassett, S. Ucar, B. L. Strand, J.-P. Andreassen, P. Sikorski, A correlative spatiotemporal microscale study of calcium phosphate formation and transformation within an alginate hydrogel matrix, Submitted to Acta Biomaterialia.

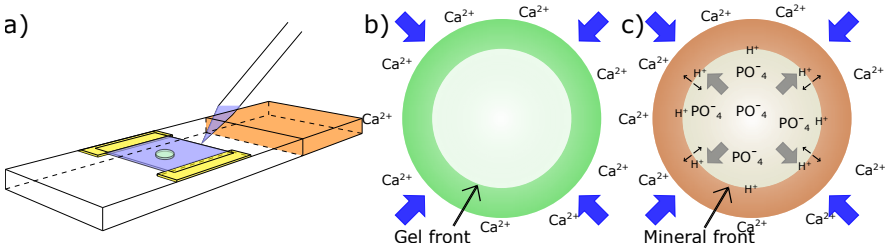

Figure 1: **(a)** Illustration of the flow cell for gelling experiments. **(b)** and **(c)** Schematic cross-sections of a gelling and mineralizing hydrogel bead or disc. The blue arrows denote calcium flux, the gray arrows denote phosphate flux, and the black arrows denote H^+ flux. The solid green color represents gelled alginate, while brown color represents mineral formation.

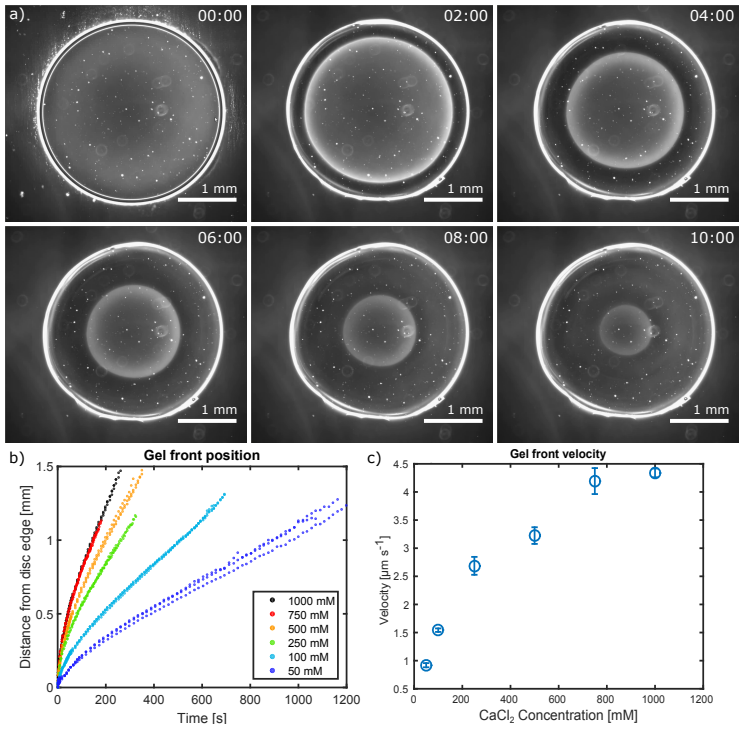

Figure 2: **(a)** Gel front position as observed by DF microscopy for gelling with 100 mM $CaCl_2$ at indicated timepoints (minutes). **(b)** Gel front position as a function of time determined from DF micrographs for $CaCl_2$ between 50 mM and 1 M showing 3 parallel experiments for each concentration. **(c)** Gel front velocity as a function of $CaCl_2$ concentration determined from the linear region.

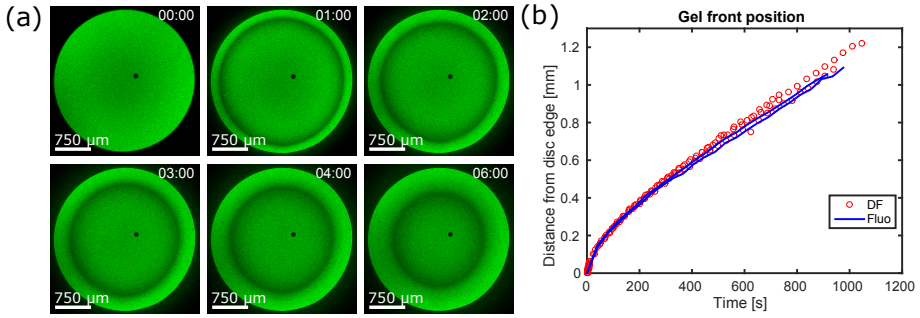

Figure 3: **(a)** Time series of alginate gelling in flow cells as determined by confocal microscopy. Brightness corresponds to the fluorescence intensity of labeled alginate and the time difference between frames is 60 s. The top left image was taken immediately before the gelling solution was added. The gel front is visible as a region with reduced fluorescence moving towards the center of the disc. **(b)** A comparison of the gel front position as a function of time as determined by CLSM and DF microscopy showing excellent correlation between the two techniques. In both (a) and (b) the concentration of gelling solution was 50 mM $CaCl_2$.

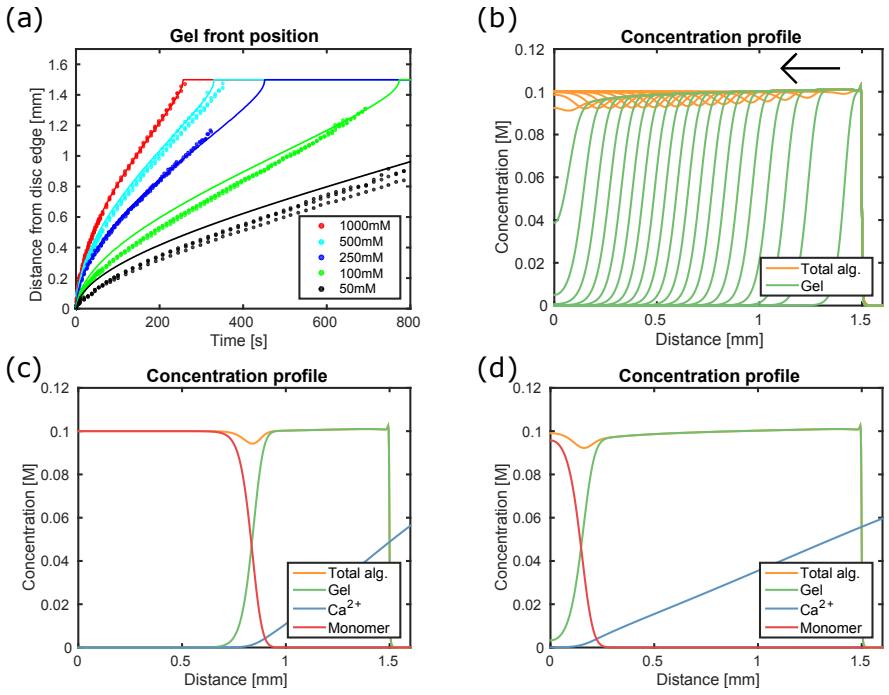

Figure 4: **(a)** A comparison of the gel front position as a function of time as determined experimentally by DF microscopy (dots) compared to model predictions (line). **(b)** Modelling of the spatiotemporal evolution of the gelled alginate concentration (gel front) calculated for 100 mM $CaCl_2$ at intervals of 40 s. The movement of the gel front is indicated by an arrow. **(c)** and **(d)** Concentration profiles for Ca^{2+} (black), ungelled (blue), gelled (red) and total alginate (i.e. ungelled + gelled, green) 240 s **(c)** and 720 s **(d)** after the gelling was initiated, calculated for a gelling solution concentration of 100 mM.

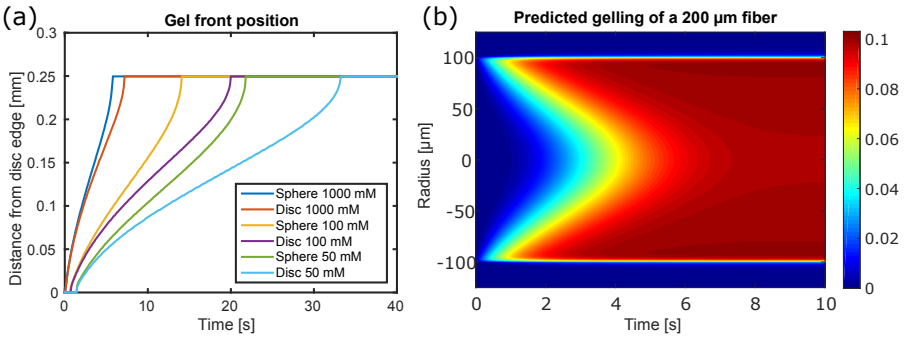

Figure 5: **(a)** The calculated gel front position as a function of time for a spherical and cylindrical geometry with radius = 250 µm for different $CaCl_2$ concentrations (50 mM, 100 mM and 1000 mM) using the proposed model.**(b)** The calculated amount of gelled alginate (between 0 and 0.1 M) for a fiber with radius = 100 µm in a microfluidic device with 100 mM $CaCl_2$. The x-axis represents time in the gelling channel.

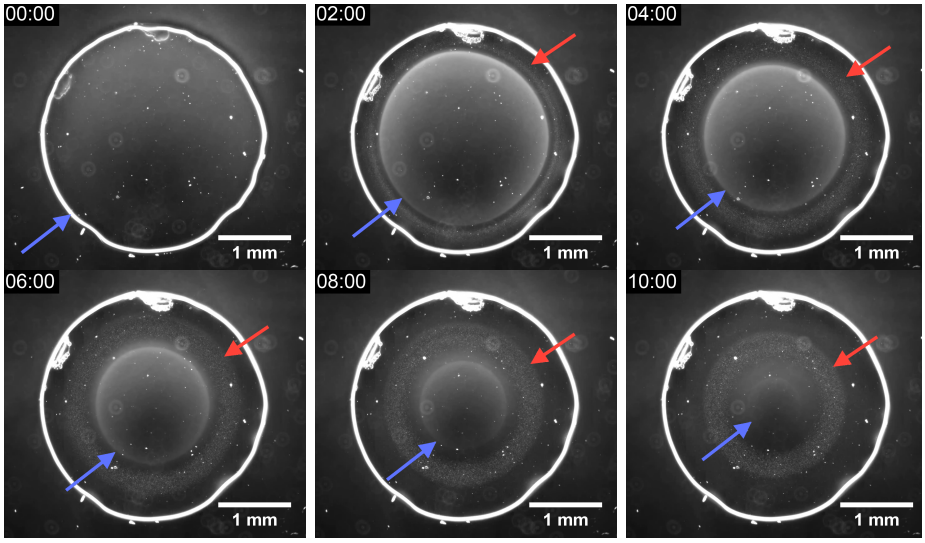

Figure 6: Gel front and mineral front position as observed by DF microscopy of a phosphate-containing alginate disc gelled with 1 M $CaCl_2$ solution. The gel front indicated by blue arrows appeared weaker and moved slower as compared to previous experiments without phosphate. A moving front of minerals indicated by red arrows trailed the gel front and widened over time. Time for each frame in minutes is shown in the top left corner.

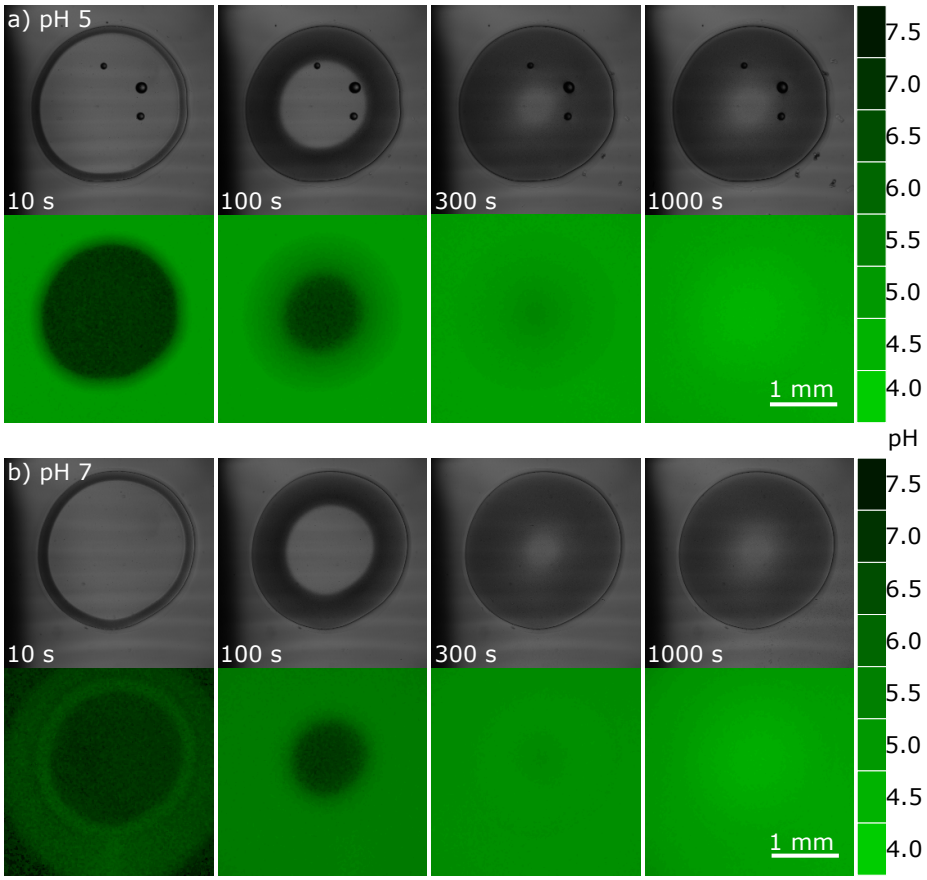

Figure 7: **a)** Bright field images (top) and pH-images (bottom) of a phosphate containing sample subjected to 1 M $CaCl_2$ buffered at pH 5. The intensity in the green images correspond to the pH given in the scale on the right. **b)** Bright field images (top) and pH-images (bottom) of a phosphate containing sample subjected to 1 M $CaCl_2$ buffered at pH 7. In both cases, the initial pH of the alginate was pH 7.

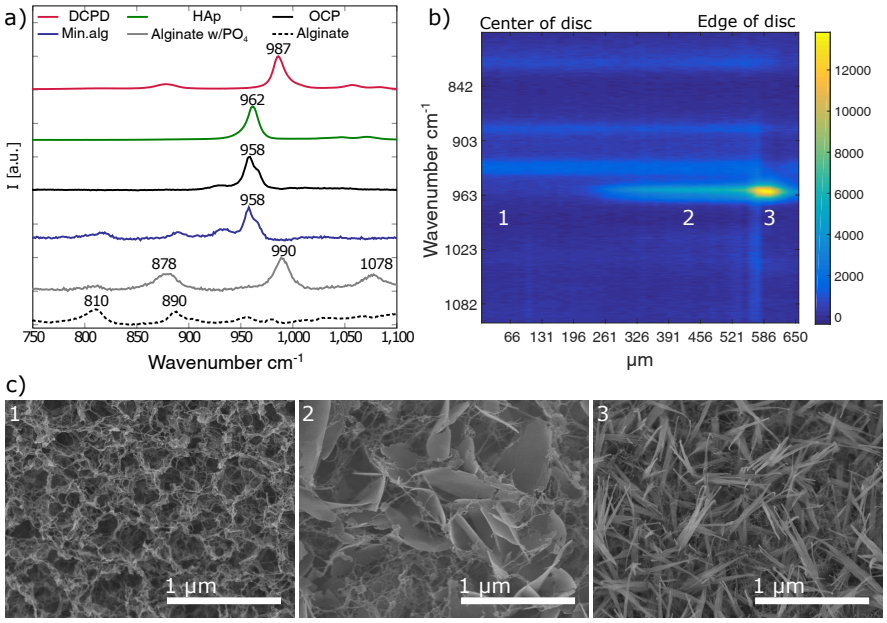

Figure 8: **(a)** Raman spectra of relevant standard samples showing typical features which can be identified. **(b)** A heat map showing the distribution of mineral from the center towards the edge of the disc. The white numbers refer to the positions of SEM-images shown in **c)**. **c)** SEM images of positions 50 µm from the center **(1)**, 450 µm from the center **(2)** and 600 µm from the center, close to the edge **(3)** of a mineralized alginate disc after 24 h in the gelling solution.